Engineering Active Sites Enriched *2D-on-1D* NiFe and NiCo Layered Double Hydroxide-Decorated Ni Nanowire Networks for Oxygen Evolution Reaction

Khaled M. Amin,* Kuan-Hsun Lin, Michael Duerrschnabel, Leopoldo Molina-Luna, and Wolfgang Ensinger

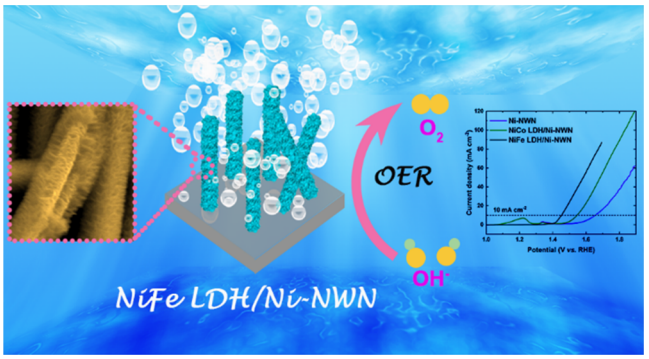

ABSTRACT: Green energy technologies, including water splitting and fuel cells, are being extensively pursued to meet the increased demand for renewable energy and tackle the pollution issues related to fossil fuel consumption. The performance of these technologies primarily relies on noble-metal-oxide electrocatalysts, which are typically supported by macroscopic and weighty materials. Therefore, it is urgently needed, although it is still challenging to engineer highly efficient an d na turally abundant electrocatalysts in micro- and nanostructures. Herein, we applied a facile strategy to fabricate highly efficient electrocatalysts based on different l ayered d ouble h ydroxides (LDHs), n amely, N iCo and NiFe, grown over a free-standing 1D Ni nanowire network (Ni-NWN) for oxygen evolution reaction (OER). Benefiting from the synergy of coupling the 2D LDH nanosheets with its high catalytic activity and the Ni-NWN with its interconnected highly conductive structure and high porosity, the as-prepared NiFe LDH/Ni-NWN exhibited excellent OER performance with a low overpotential of only 222 mV to deliver 10 mA cm^{-2}. Furthermore, it revealed favorable kinetics, in terms of a 42 mV dec^{-1} Tafel slope and a low charge transfer resistance. The 3D architecture with its "nanosheet on nanowire" structure improves the mechanical stability, besides retaining efficient electron paths through the Ni-NWN and high ionic diffusion rates through the porous network, which in turn promotes the generation of active phases during OER and provides outstanding durability over 50 h. Furthermore, the architectures' proposed strategy and flexible e ngineering a re h ighly p romising a nd c ould b e a dopted t o f abricate other electrocatalysts for widespread applications.

KEYWORDS: *Track-etched membranes, Layered double hydroxides, Nanowire arrays, Hierarchical structures, Electrodeposition, Self-supported electrodes, OER*

INTRODUCTION

The relentless pursuit of sustainable energy solutions, aimed at meeting the growing energy demand while mitigating the environmental concerns arising from the utilization of fossil fuel, is a high-priority international target and comes on top of the current research topics.[1−5] Different approaches have been implemented to maximize the market share of renewable energy systems, including energy conversion and storage systems e.g. fuel cells, water splitting, and metal−air batteries.[6−8] As a sustainable and green energy resource, hydrogen represents the major player that can change the future of the energy market.[9] Water splitting is seen as the most promising and scalable strategy for the production of green hydrogen. This process mainly involves two reactions: (i) hydrogen evolution, which occurs at the cathode, and (ii) oxygen evolution, which occurs at the anode. Nevertheless, the OER is commonly regarded as the bottleneck within the water splitting mechanism. This is because the OER encompasses several proton-coupled electron transfer steps that are inherently slow kinetically, subsequently impacting the overall efficiency of the water splitting process.[10,11] Even the commonly used noble metal-based electrocatalysts (RuO_2 and IrO_2) necessitate a high overpotential to overcome the energy barrier essential for the OER.[12] Also, the limited availability and high production costs associated with noble metals impose constraints on the widespread implementation of such catalysts on a large scale. Hence, extensive research is

currently being focused on designing abundant and cost-effective transition metal-based electrocatalysts as alternatives with high activity toward OER.[9,13]

Transition metal-based electrocatalysts represent promising competitors that can replace noble metal-based ones, including oxides, hydroxides, sulfides, nitrides, and phosphides.[13−20] Among these materials, LDHs have emerged as a highly promising class capable of meeting the majority of the criteria for effective electrocatalysts in alkaline media due to their distinguished 2D structure with interlayer spaces, large active surface areas, and tunable compositions.[21,22] NiFe LDH is regarded as highly efficient as an electrocatalyst in alkaline media due to its ability to facilitate the OER process with a low overpotential.[23−25] Several studies have been conducted to further enhance the NiFe-LDH activity toward the OER. However, developing an ideal electrocatalyst for the OER is not yet accomplished. Most LDHs have low conductivity, as they are insulators or semiconductors, which severely affects the OER activity. Additionally, they tend to agglomerate.[26]

Various approaches have been proposed to address these challenges and boost the performance of LDH-based electrocatalysts, such as hybridization, modulating the electronic structure, intercalating, and nanostructuring.[27−31] The engineering of electrocatalysts with nanoscale architectures is gaining increasing attention.[32,33] This approach aims to maximize catalyst efficiency by increasing the surface area and enhancing the mass and charge transfer. Consequently, it provides better accessibility to active sites, leading to improved performance. One-dimensional (1D) nanowire networks such as Ni-NWN can offer a platform with highly conductive pathways for electron transfer working as a backbone that carries the active material. The overall 3D architecture, which consists of a *2D-on-1D* core−shell structure, merges the advantages of 1D Ni-NWN with its porous structure, namely, the high conductivity and the mechanical stability, with those of the 2D LDH nanosheets which act as a shell layer with high redox catalytic activity and great surface area. Additionally, the direct contact between the LDH layer and interconnected Ni nanowires plays a crucial role in accelerating charge transfer. This can be attributed to the robust connection between the LDH layer and Ni-NWN, where each Ni nanowire acts as an individual current collector. The proposed hierarchical structure provides multiple advantages over the common bulk composites due to the synergy between the individual components in such a multilevel hierarchy.

Numerous studies have reported the utilization of NiCo and NiFe LDH-based electrocatalysts for OER, employing different shapes, such as nanosheets, nanotubes, and nanowires, which establish direct contact with the current collector.[34−38] However, the geometry and dimensions of such electrodes are mainly correlated to the dimensions of the parent substrate, which carries the active material and works as a supporting electrode such as foams, felts, and cloths. Most of these substrates have dimensions in the microscale, which limit the active surface area of the electrode and restrict their use in certain applications that require an electrode of smaller thickness or lower mass. Meanwhile, nanowire networks provide an extra striking feature, namely, the nanoscale dimensions and the straight orientation, which can dramatically boost the performance of the electrocatalyst besides the common characteristics shared with the other common substrates, including the porous intersected structure. Accordingly, it is essential to establish a rational synthetic approach to create a cost-effective electrocatalyst that meets the criteria for achieving a high OER performance. Designing a nanoscale architecture overgrown by various electrocatalytic active materials of varying dimensionality can effectively address many functionality issues, including better exposure of the active sites, higher conductivity, and faster diffusion rates of ions through these nanoreactors.[28,39]

Inspired by these considerations, herein, we highlighted a new fabrication strategy of self-supported 3D hierarchical NiCo LDH/Ni-NWN and NiFe LDH/Ni-NWN electrocatalysts with a core−shell structure via facile in situ electrodeposition of LDH nanosheets over Ni-NWN. The free-standing Ni network was obtained through a template-assisted strategy to deposit Ni inside the pores of commercial track etched membranes, forming a self-supported network that acts as a substrate and current collector without needing a binder or conductive material. As such, LDH nanosheets serve as the active material; this coating delivers high electrocatalytic activity through its abundant active sites and excellent stability, while the 3D NWN provides mechanical strength, large surface areas, and high electron conductivity. Furthermore, the 3D self-supported electrodes offer a higher diffusion rate of ions through their tortuous structure. The introduced approach employs scalable and simple techniques that can be customized to prepare a variety of architectures with different compositions and ratios of active materials. Three electrodes (Ni-NWN, NiCo LDH/Ni-NWN, and NiFe LDH/Ni-NWN) have been examined as electrocatalysts for OER. NiFe LDH/Ni-NWN required a very low overpotential of 222 mV to attain 10 mA cm^{-2}, all while retaining outstanding stability over a 50 h duration. Moreover, it possessed a lower charge transfer resistance (R_{ct}) and smaller Tafel slope compared to Ni-NWN and NiCo LDH/Ni-NWN, delivering a better overall electrocatalytic performance. This performance even outperforms most recently reported transition metal-based electrocatalysts. Considering its impressive OER performance, stability, and the abundant availability of LDH metals, as well as the feasible and scalable synthetic approach, it is anticipated that the NiFe LDH/Ni-NWN electrocatalyst presented here holds significant potential to replace noble-metal-based catalysts in real-world applications for OER.

EXPERIMENTAL SECTION

Materials. Polycarbonate template membranes had the following specifications: a thickness of 25 μm, a pore diameter of 400 nm, and a pore density of 1.5×10^8 cm^{-2} (ipPORE from it4ip). The following chemicals were utilized as received: boric acid (H_3BO_3, 99.5%, Sigma), nickel chloride ($NiCl_2$, 98%, Aldrich), nickel nitrate hexahydrate ($Ni(NO_3)_2{\cdot}6H_2O$, GR, Merck), dichloromethane (CH_2Cl_2, puriss. p.a., Sigma-Aldrich), iron sulfate heptahydrate ($FeSO_4{\cdot}7H_2O$, ≥ 99%, Sigma-Aldrich), cobalt nitrate hexahydrate ($Co(NO_3)_2{\cdot}6H_2O$, 99+%, Acros Organics), and KOH (Sigma-Aldrich). Deionized water was employed in all procedures.

Synthesis of Ni-NWN. To prepare the free-standing Ni-NWN electrodes, a template-assisted electrodeposition method was employed. Briefly, ion track-etched membranes were first sputtered with a thin Ni layer under a current of 100 mA for 180 s to provide conductivity to the template. The sputtered template was then subjected to electrodeposition within a three-electrode setup to reinforce the electrode and retain mechanical stability. The electrodeposition process took place in an electrolyte solution containing 0.5 M $NiCl_2$ and 0.5 M H_3BO_3. A constant potential of −0.9 V vs. Ag|AgCl was applied during this process, with the thickness of the Ni supporting layer being regulated by maintaining an accumulated charge of 100 C. In order to obtain the free-standing Ni-NWN, the

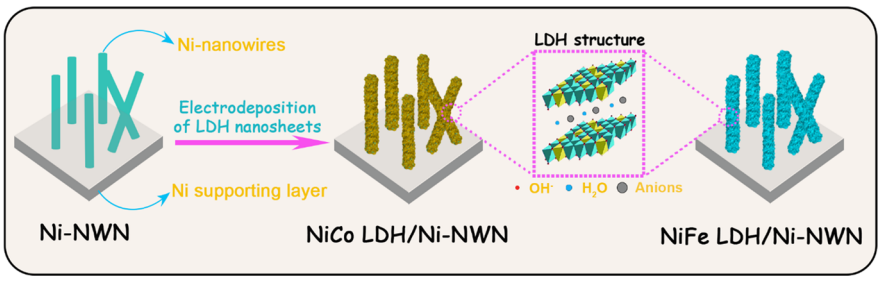

Figure 1. Schematic illustration of the fabrication process of the free-standing NiCo LDH/Ni-NWN and NiFe LDH/Ni-NWN architectures.

same electrodeposition parameters and the same electrolyte were employed to deposit Ni until the pores of the template were filled. The upper side of the template was then carefully polished with aqua regia to eliminate any extra deposition over the template surface. Finally, the template was immersed in dichloromethane to dissolve the polymer matrix and then cleaned with deionized water.

Synthesis of Core/Shell-like NiCo and NiFe LDH-Decorated Ni-NWN. NiCo and NiFe LDH nanosheets were directly grown over Ni-NWN via pulsed potential electrodeposition. For NiCo LDH, an electrolyte containing a 1:1 molar mixture of 0.05 M $Ni(NO_3)_2{\cdot}6H_2O$ and 0.05 M $Co(NO_3)_2{\cdot}6H_2O$ was used. The pulsed electrodeposition process involved applying −1 V vs. Ag|AgCl with intermittent pulses of 1 V vs Ag|AgCl for 0.5 s every 3 s. This process was carried out for a duration of 90 s. Subsequently, the samples underwent thorough washing with H_2O and were dried. Similarly, for NiFe LDH, an electrolyte containing 0.15 M $Ni(NO_3)_2{\cdot}6H_2O$ and 0.15 M $FeSO_4{\cdot}7H_2O$ was employed, and the pulsed electrodeposition was conducted using the same parameters.

Surface and Structural Characterization. Scanning electron microscopy (SEM) measurements were conducted by using a Philips XL30 FEG instrument (Netherlands), operating at acceleration voltages ranging from 10 to 30 kV. X-ray diffraction (XRD) analysis was achieved with a D8 Advance diffractometer (AXS Bruker, Germany) supplied with a Cu anode and utilized Bragg−Brentano geometry along with an SOL X Detector. Additionally, a Seifert XRD 3003 PTS-3 instrument was used with monochromated Cu Kα radiation. The recorded spectra spanned the range of 2θ = 8−90°, with a step size of 0.02° for the complete spectrum and 0.03° for the highlighted areas of interest, employing a slower scan speed. The full spectra were recorded with a scan speed of 2θ = 250 s^{-1}, while the areas of interest highlighted in the XRD figure were scanned with a slower scan rate of 2θ = 1666 s^{-1}. Transmission electron microscopy (TEM) images and selected area electron diffraction (SAED) patterns were accumulated with a Thermofisher Talos F200X equipped with a Ceta CCD camera, a SuperX energy-dispersive X-ray (EDX) detection system, and a Gatan Enfinium electron energy-loss spectroscope. The microscope operated at an acceleration voltage of 200 kV. Data analysis for TEM was conducted using Thermofisher Velox, Digital Micrograph, and SingleCrystal[40] softwares. To analyze the composition and elemental oxidation states of the three electrodes, X-ray photoelectron spectroscopy (XPS) was employed, utilizing a SPECS PHOIBOS 150 (Germany). A monochromatized Al Kα line with an excitation energy of 1486.7 eV was employed as the X-ray source. CasaXPS (version 2.3.25) was employed to fit the acquired spectra and subtract the background using the Shirley method.[41] For consistency, the spectra were calibrated by setting the C 1s peak at 284.5 eV.

Electrochemical Experiments. The electrodeposition experiments were conducted in a three-electrode setup using a Keithley 2602 System SourceMeter unit (USA). Sputtered polymer templates served as the working electrodes (WE), while Ag|AgCl functioned as the reference electrode (RE), and a Pt spiral electrode acted as the counter electrode (CE). The deposition of NiCo and NiFe LDH nanosheets was achieved using the previously prepared Ni-NWN as the WE, following the same conditions. Electrochemical measurements were carried out in a custom-designed three-electrode setup utilizing a Gamry Reference 600 potentiostat (USA). The reference electrode employed was Hg|HgO filled with 1 M KOH, the counter electrode was a Pt spiral wire, and the working electrode was a round, free-standing sample with a diameter of 13 mm of the three electrocatalysts (Ni-NWN, NiCo LDH/Ni-NWN, and NiFe LDH/Ni-NWN). All of the experiments were conducted in a 1 M KOH solution as an electrolyte. Potentials were converted to a reversible hydrogen electrode (RHE) scale using the formula:

$$E_{RHE} = E_{Hg/HgO} + 0.059{\cdot}pH + 0.98$$

Before the electrocatalytic performance was assessed, the electrocatalysts were activated by running cyclic voltammetry under a scan rate of 50 mV s^{-1} until reaching a steady state of each electrocatalyst. The activity toward the OER was investigated by linear sweep voltammetry (LSV) at a scan rate of 1 mV s^{-1}, and Tafel slopes were calculated from LSV. Overpotential was calculated using the following equation:

$$\eta(\mathrm{V}) = E_{RHE} - 1.23$$

Electrochemical impedance spectroscopy (EIS) was conducted over a frequency range spanning from 0.01 Hz to 100 kHz, using an amplitude of 10 mV (NiFe LDH@Ni-NTNW was represented within the frequency range of 0.5 Hz to 100 kHz for improved fitting). Durability was assessed through chronopotentiometry (CP) performed at a current density of 10 mA cm^{-2} for 50 h.

RESULTS AND DISCUSSIONS

Characterization of the Hierarchical Architectures. In contrast to the traditional methods for synthesizing electrocatalysts, the innovative approach employed in creating hierarchical NiCo LDH/Ni-NWN and NiFe LDH/Ni-NWN architectures (Figure 1) represents a feasible and scalable pathway for establishing a flexible model of self-supported electrodes. This model can be adopted to functionalize NWN-based platforms with various active materials, suitable for diverse catalytic applications. The synthesis process began with the electrodeposition of Ni-NWN within the pores of the polymer template on the back sputtered Ni layer. Subsequently, the NiFe LDH and NiCo LDH nanosheets were grown over the core Ni-NWN via controlled pulsed electrodeposition, forming the hierarchical core−shell architectures. Hierarchical architectures, in contrast to bulk materials, exhibit remarkable synergistic effects arising from the combined properties of their individual components within a multilevel structure. It is crucial to emphasize that our 3D porous structure provides a significantly larger interior surface area when compared to conventional substrates like Ni foams or fibers. This synthetic approach offers an integrated and robust design of the catalyst electrode, capitalizing on the extensive surface area and excellent catalytic activity of the 2D LDH nanosheets, as well as the high electrical conductivity, mechanical strength, and efficient electron transfer pathways of the 1D Ni-NWN. The interplay between these components in our hierarchical architecture not only facilitates enhanced

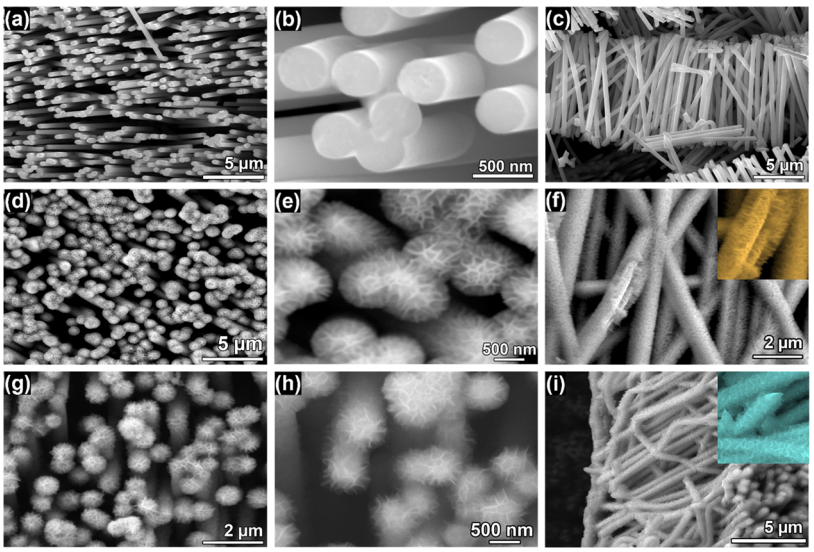

Figure 2. Top-view and side-view SEM of (a–c) Ni-NWN, (d–f) NiCo LDH/Ni-NWN, and (g–i) NiFe LDH/Ni-NWN.

activity but also enables easy handling of the electrode without the need for supporting electrodes or binders, retaining the mechanical stability of the stand-alone network without any damage.

Surface and structural analyses of the electrodes confirmed the successful optimization of the deposition parameters. SEM micrographs of Ni-NWN (Figure 2a–c) depicted the conformal deposition of Ni inside the entire pores of the parent templates, creating coherent and uniform Ni nanowires with a diameter of approximately 400 nm, closely mirroring the original nanopore diameter. After the polymer template was dissolved, the as-prepared nanowire network preserved a self-supported architecture growing over the electrodeposited Ni supporting layer, which works as a current collector for this electrode, as represented in Figure S1. As for this paradigm, the Ni-NWN acts as a 3D conductive core, which is efficiently connected to a thin layer of Ni that retains the network integer and provides a conductive pathway to the potentiostats. The top view of Ni-NWN (Figure 2b) depicts the intersections between the wires, which retain the structure intact and prevent stacking of the wires. The lateral view of prepared Ni-NWN (Figure 2c) reveals the free-standing architectures, which appear free from any polymer residuals while maintaining an intact structure. The resulting 3D interconnected nanowire network serves as a perfect conductive scaffold for the subsequent growth of the NiCo and NiFe LDH nanosheets. These LDH nanosheets were erectly deposited onto the Ni-NWN, creating a well-defined hierarchical "nanosheet on nanowire" architecture. In the case of the NiCo LDH/Ni-NWN architecture, as illustrated in Figure 2d–f, the NiCo LDH nanosheets forming the outer layer on the Ni-NWN backbone exhibit a distinct wrinkled structure, which sets them apart. The side view of the network (Figure 2f) provides confirmation that the entire length of the nanowires is uniformly coated with a consistent layer of NiCo LDH nanosheets. Similarly, the SEM micrographs of the NiFe LDH/Ni-NWN electrode (Figure 2g–i) depict the Ni-NWN skeleton decorated with a layer of NiFe LDH nanosheets. As displayed in Figure 2i, the interconnected network appears to be entirely covered with LDH while retaining the porous construction of the network. This ensures that the micro pathways remain free without clogging arising from over-deposition. This approach is optimal for obtaining a significant amount of active material (NiCo or NiFe LDH), thereby enhancing the catalytic activity of the electrodes while allowing for the unimpeded diffusion of the electrolyte through the catalysts.

The hierarchical design of the catalysts was further investigated by using TEM accompanied by SAED on cross sections of the prepared composites. TEM images of the Ni-NWN catalyst (Figure 3a) showed circular-shaped Ni wires with uniform morphology and a diameter of approximately 400 nm along the entire wire length. The SAED pattern displayed diffraction rings (Figure 3b,c), indicating the polycrystalline nature of the Ni-NWN with characteristic ring patterns corresponding to the (111), (200), (220), (400), and (420) crystal planes. To validate the synthetically projected core–shell structure of the coated nanowires, TEM analysis was performed on NiCo LDH/Ni-NWN (Figure 3d) and NiFe LDH/Ni-NWN (Figure 3g). Both catalysts exhibited a uniform coating layer composed of plentiful flaky nanosheets surrounding the Ni-NWN skeleton which appeared darker compared to the surrounding NiCo LDH and NiFe LDH nanosheets, as depicted in Figure 3d,g, respectively. Further, local SAED measurements were conducted at different spots representing the Ni core and the shell layer of NiCo LDH and NiFe LDH nanosheets, as marked by the dashed circles in Figure 3d,g. SAED analysis of NiCo LDH/Ni-NWN and NiFe LDH/Ni-NWN revealed the same characteristic rings of polycrystalline Ni at the centers of the wires (Figure 3e,h), dominated by the Ni core. In contrast, the SAED obtained from the shell layer, where the NiCo LDH and NiFe LDH nanosheets have been deposited (Figure 3f,i, respectively), revealed the characteristic continuous rings of the amorphous LDH structure with ring patterns of (0003), (0006), (1102), (1105), and (11010) planes. EDX mapping images of Ni-NWN (Figure S2) confirmed that Ni was the major element present in the wires. Elemental mapping was further conducted on NiCo LDH/Ni-NWN (Figure S3) and NiFe LDH/Ni-NWN (Figure 3j) to elucidate the spatial distribution of elements throughout the heterostructure of the catalysts. As shown in Figure 3j, the EDX mapping images demonstrated a

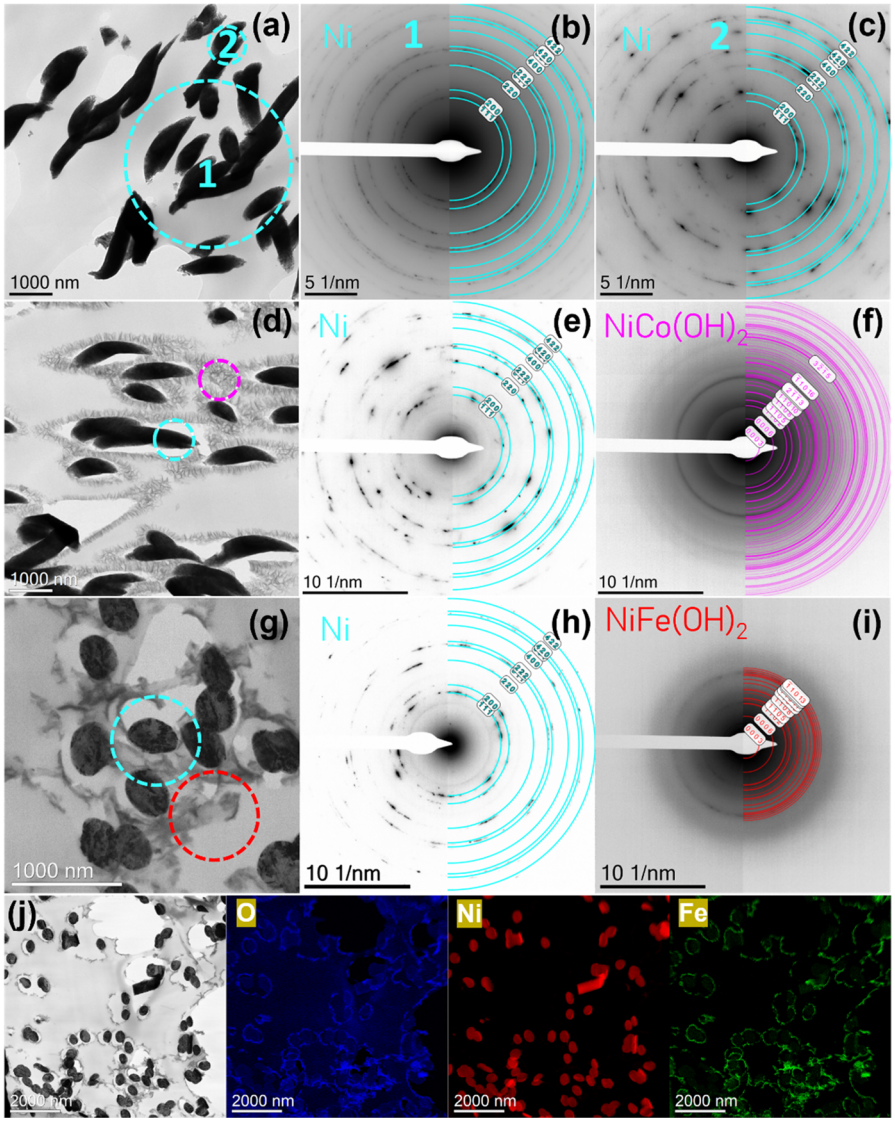

Figure 3. TEM images of (a) Ni-NWN, (d) NiCo LDH/Ni-NWN, and (g) NiFe LDH/Ni-NWN. SAED of (b, c) Ni-NWN, (e, f) NiCo LDH/Ni-NWN, and (h, i) NiFe LDH/Ni-NWN conducted at different spots highlighted with circles in the TEM micrographs (a), (d), and (g), respectively. (j) EDX mapping images of the NiFe LDH/Ni-NWN catalyst.

concentrated distribution of Ni in the core, whereas elemental Fe and O were uniformly dispersed within the NiFe LDH shells, aligning with the intended heterostructure design. Such a hierarchical "nanosheet on nanowire" architecture, benefiting from the added LDH layer, not only provides an abundance of redox-active sites due to its expanded surface area but also promotes efficient electrolyte diffusion through its open porous structure. As a result, these architectures exhibit an enhanced electrocatalytic performance.

XRD analysis of as-synthesized Ni-NWN, NiCo LDH/Ni-NWN, and NiFe LDH/Ni-NWN was conducted to provide more structural information about the crystalline structure. The XRD pattern of Ni-NWN (Figure 4a) revealed the major diffraction peaks at 44.6°, 51.8°, and 76.4°, which match well to the (111), (200), and (220) planes, respectively, of metallic Ni (JCPDS No. 04-0850).[28] Besides the characteristic peaks of the Ni nanowires, the XRD patterns of NiCo LDH/Ni-NWN and NiFe LDH/Ni-NWN exhibited several discernible diffractions with low intensities, which become more apparent at slower scan speeds (highlighted regions in Figure 4a) at 2θ values of 10.5°, 22.6°, 34.4°, and 60.7°. These reflexes could be attributed to the (003), (006), (012), and (110) planes of the hydrotalcite-like LDH phase (JCPDS 33-0429 and JCPDS 40-0215), which agrees with the crystallographic data acquired from SAED measurements.[33,42,43] The low intensity of these peaks may be related to the existence of the NiCo and NiFe LDH sheets in a nanoscale ultrathin structure with poor crystallinity; such weak peaks were buried by the stronger characteristic peaks of Ni-NWN.[42]

The chemical and structural compositions and elemental valence states of the prepared catalysts were further investigated using XPS. As shown in Figure 4b, the survey spectrum of NiCo LDH/Ni-NWN revealed the existence of Ni, Co, and O, and that of NiFe LDH/Ni-NWN confirmed the existence of Ni, Fe, and O, while no Co or Fe signals were present in the spectrum of Ni-NWN, which agree with the EDX results (Figures 3j, S2, and S3). The Ni 2p spectra of NiCo LDH/Ni-NWN and NiFe LDH/Ni-NWN (Figure 4c) revealed two peaks around 855.6 eV (Ni $2p_{3/2}$) and 873.4 eV (Ni $2p_{1/2}$) along with two shakeup satellite peaks (861.6 and

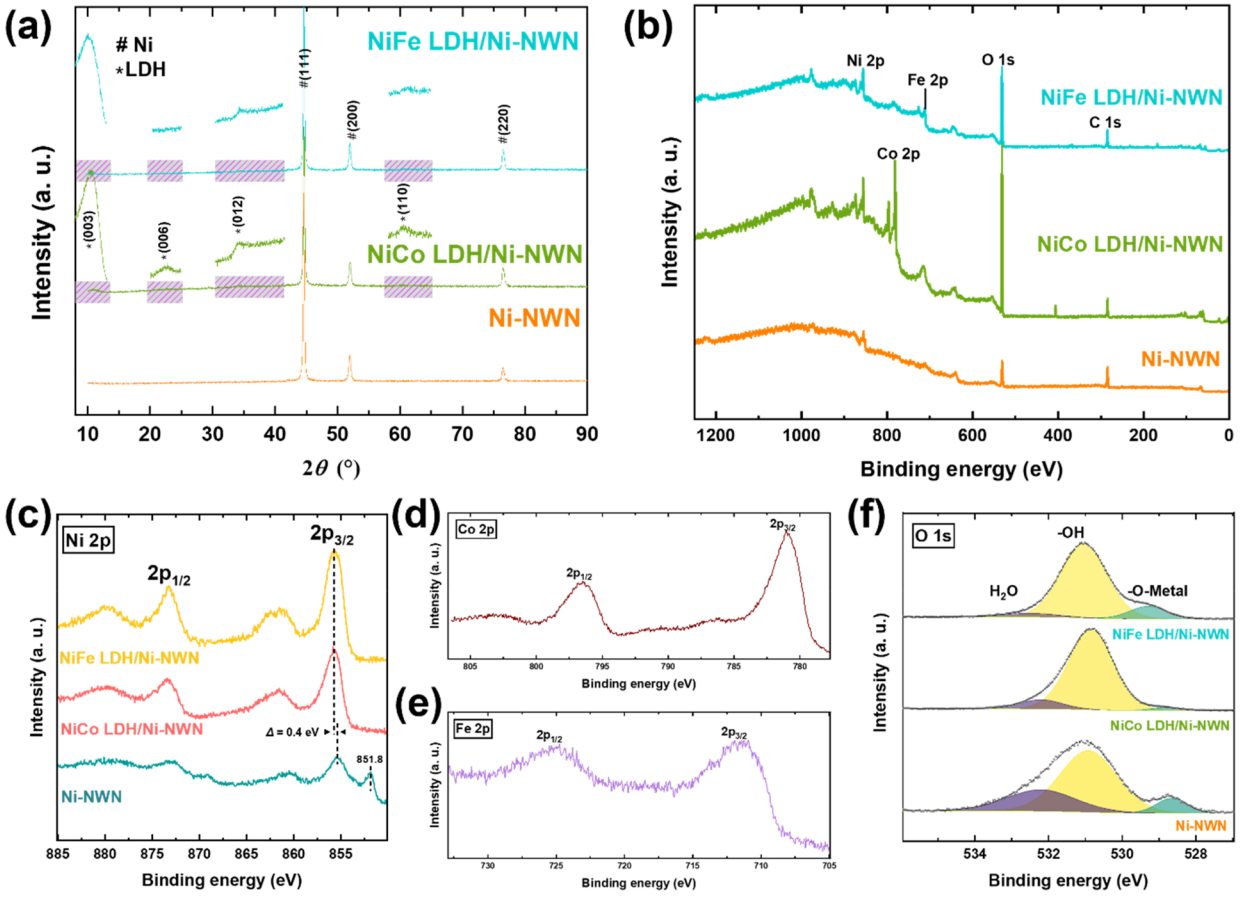

Figure 4. (a) XRD patterns (highlighted insets show the characteristic peaks of LDH under slow scan rate) and (b) XPS survey scans of Ni-NWN, NiCo LDH/Ni-NWN, and NiFe LDH/Ni-NWN. High-resolution XPS spectra of (c) Ni 2p region of the three catalysts, (d) Co 2p region of NiCo LDH/Ni-NWN, and (e) Fe 2p region of NiFe LDH/Ni-NWN and (f) O 1s XPS spectra of the three electrodes.

879.7 eV) which are indicative of the $Ni(OH)_2$ phase as reported in the previous studies.[44,45] At the same time, Ni-NWN showed extra peaks at 851.8 and 869.1 eV, which are characteristic of Ni^0, emanating from the underlying nanowire network. These two peaks disappear upon the deposition of the surface LDH layer over the core metal, as observed in the case of NiCo LDH/Ni-NWN and NiFe LDH/Ni-NWN. Furthermore, in comparison to Ni-NWN, the Ni $2p_{3/2}$ and Ni $2p_{1/2}$ peaks in NiCo LDH/Ni-NWN and NiFe LDH/Ni-NWN are shifted to higher binding energy by approximately 0.4 eV. This shift is attributed to the electron transfer from the Ni d band to the Co d and Fe d bands, indicating a strong interaction between Co and Fe ions with Ni ions in NiCo LDH/Ni-NWN and NiFe LDH/Ni-NWN, respectively.[46] In the high-resolution Co 2p region, two binding peaks at approximately 781 and 796.4 eV, along with satellite peaks, as illustrated in Figure 4d, are indicative of the characteristic behavior of $Co(OH)_2$.[47] The Fe 2p spectrum, as shown in Figure 4e, exhibits two distinct peaks at approximately 711.4 and 725.1 eV, corresponding to Fe $2p_{3/2}$ and Fe $2p_{1/2}$, respectively. This suggests the presence of Fe species in a +3 oxidation state within NiFe-LDH/Ni-NWN.[44] The O 1s spectrum of the three composites (Figure 4f) reveals two main peaks assigned to M−O (Ni−O, Co−O, and Fe−O) species at 528.7−529.3 eV and M−OH species at 531.4 eV.[42] The findings from the XPS measurement confirm the existence of Ni, Co, and Fe in multiple oxidation states within the NiCo and NiFe LDH nanosheets. These solid-state redox couples, including Ni^{2+}/Ni^{3+}, Fe^{2+}/Fe^{3+}, and Co^{2+}/Co^{3+}, are known to contribute significantly to electrochemical activity, particularly because Ni^{3+}, Fe^{3+}, and Co^{3+} represent catalytically active sites toward OER. Moreover, the Ni^0 peak disappeared in the case of NiCo LDH/Ni-NWN and NiFe LDH/Ni-NWN due to the coverage of the core Ni network.

Oxygen Evolution Reaction Performance. To assess the OER activity, the performance of hierarchical architectures was evaluated by using a typical three-electrode system in a 1 M KOH electrolyte. The performance of the architectures was evaluated based on three key parameters: (1) overpotential, (2) Tafel slope, and (3) long-term stability. Figure 5a depicts the polarization curves of the three catalysts at a scan rate of 1 mV s^{-1}. Upon analysis, it is evident that the peak potential for Ni^{2+} oxidation into Ni^{3+} shifts from 1.33 V vs. RHE for Ni-NWN to 1.22 V vs. RHE for NiCo LDH/Ni-NWN. This shift indicates that the presence of Co facilitates the $Ni^{2+/3+}$ transition at lower potentials. This phenomenon can be attributed to a charge transfer process from Co to the neighboring Ni atoms within the lattice. The charge transfer is influenced by Ni's higher electronegativity, leading to a greater charge density in Ni compared to Co.[48] Additionally, another peak, corresponding to the oxidation of Co^{3+} ions into Co^{4+} ions, is observed at 1.34 V vs. RHE. Conversely, this potential increases in the case of NiFe LDH/Ni-NWN and the transition occurs at 1.38 V vs. RHE, which nearly overlaps with the onset of the OER, indicating that the presence of Fe stabilizes the Ni^{2+} oxidation state. The inclusion of Fe

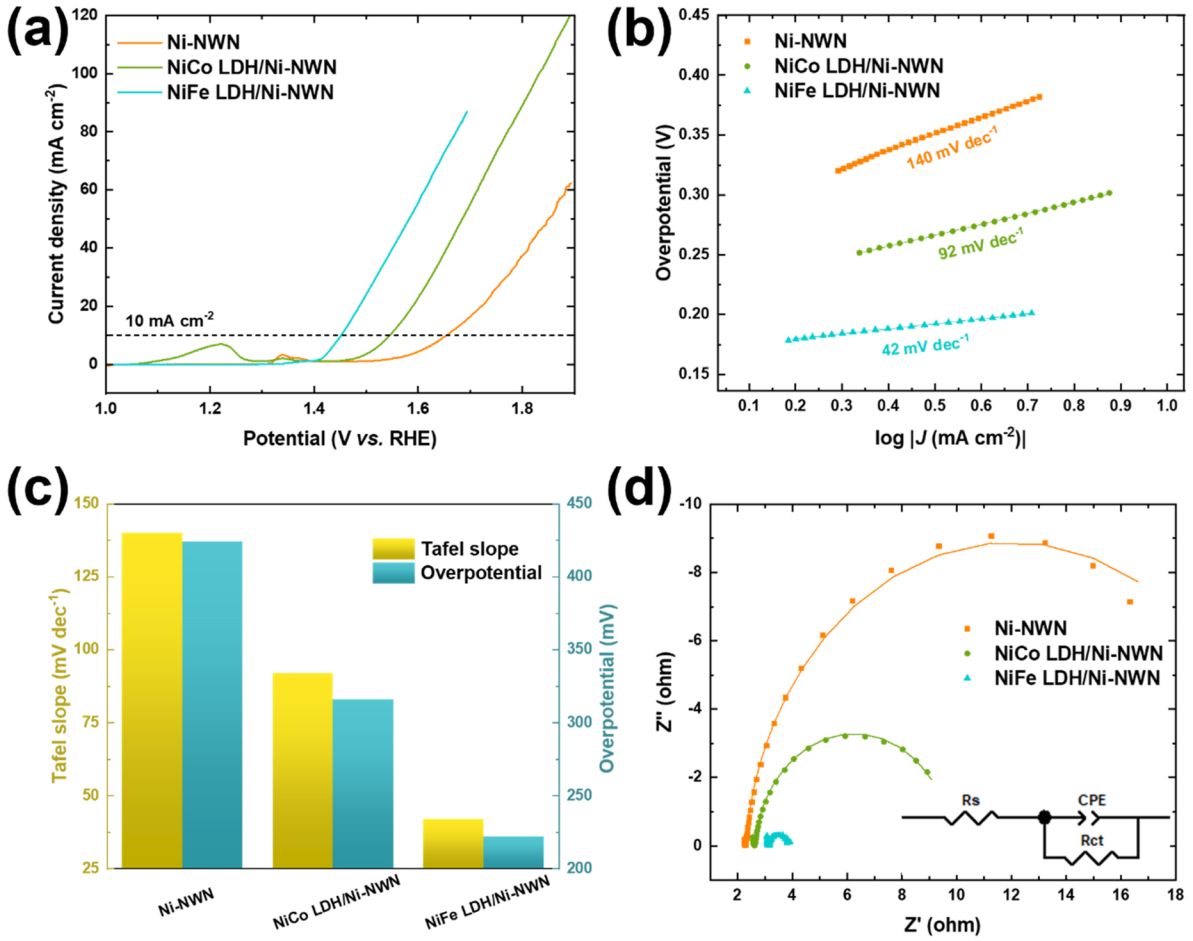

Figure 5. (a) Polarization curves of Ni-NWN, NiCo LDH/Ni-NWN, and NiFe LDH/Ni-NWN at a scan rate of 1 mV s^{-1} in 1 M KOH. (b) The corresponding Tafel plots. (c) Performance comparison of Tafel slope and overpotential at 10 mA cm^{-2} for different electrocatalysts. (d) Nyquist plots of the electrodes at a potential of 1.5 V vs RHE; inset: the corresponding equivalent circuit.

contributes to the creation of more disorders within the local structure, a characteristic associated with α-$Ni(OH)_2$.[49,50] These observations match with the previous literature, which confirms that the introduction of Fe into Ni films leads to a reduction in the average oxidation state of Ni, as opposed to pure Ni oxides. This corroborates that the presence of Fe induces an anodic shift in the $Ni^{2+/3+}$ redox pair.[51] This shift can be attributed to the relatively greater ionic character of Fe−O bonds in comparison to Ni−O. As Fe ions become incorporated into their lattice, Ni−O acquires increased covalent character. This augmented covalent nature in Ni−O demands additional potential for their electrochemical oxidation.[52] The LSV showed a lower onset potential of 1.41 V vs. RHE for NiFe LDH/Ni-NWN, which is far below 1.49 V vs. RHE of NiCo LDH@ Ni-NWN, and 1.58 V vs. RHE of Ni-NWN. The negative shift of the onset potential for the LDH-decorated networks reflects faster OER kinetics. The remarkable catalytic activity of the NiFe LDH/Ni-NWN electrocatalyst is evident from the significantly lower overpotential required to achieve a current density of 10 mA cm^{-2} (η_{10}), as marked by the dotted horizontal line in Figure 5a. The NiFe LDH/Ni-NWN exhibits an η_{10} of only 222 mV, surpassing the performance of both NiCo LDH/Ni-NWN (316 mV) and Ni-NWN (424 mV). Moreover, even at a higher current density of 100 mA cm^{-2}, the NiFe LDH/Ni-NWN retained a low η_{100} of only 487 mV, which is approximately two-thirds that of the NiCo LDH/Ni-NWN (601 mV) as demonstrated in Figure S4. In the quest for the OER kinetics, Tafel plots were constructed based on the polarization curves of the three electrocatalysts as represented in Figure 5b. The NiFe LDH/Ni-NWN exhibited a notably smaller Tafel slope of 42 mV dec^{-1} compared to 92 mV dec^{-1} for NiCo LDH/Ni-NWN, and 140 mV dec^{-1} for Ni-NWN. These results solidify that the NiFe LDH/Ni-NWN not only offers the lowest overpotential required to initiate the OER but also provides the most favorable OER kinetics among the three electrocatalysts (Figure 5c). Furthermore, to evaluate the electrochemically active surface area (ESCA) of the electrocatalysts, we calculated the double-layer capacitance (C_{dl}) based on the cyclic voltammetry curves obtained in the non-Faradaic region (Figure S5). Figure S6 shows a linearity between the capacitive current and the scan rate. Ni-NWN revealed a higher C_{dl} value (3.37 mF cm^{-2}). Interestingly, despite the highest OER activity observed for NiFe LDH/Ni-NWN, it displayed a lower ECSA compared to that of bare Ni-NWN, ruling out that ECSA is not the main parameter that drives the activity. However, determining ECSA for LDH based on C_{dl} is challenging due to the potential-dependent conductivity of LDHs, which requires good electronic conductivity to obtain reliable C_{dl} data.[53] In addition, the possible pseudocapacitive nature of the NiFe materials could lead to misleading results when using the C_{dl} method to estimate the real active surface area. Moreover,

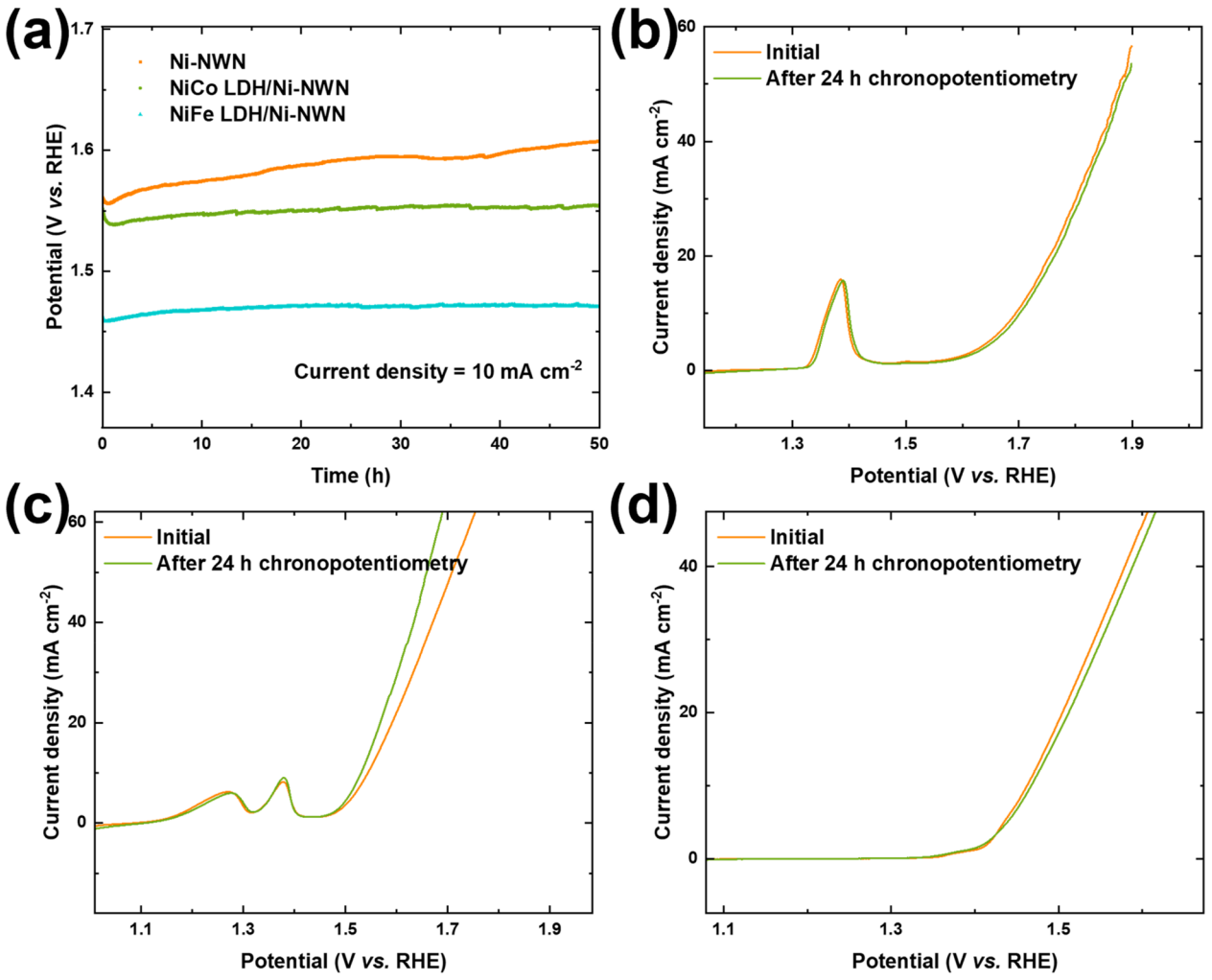

Figure 6. (a) Chronopotentiometry of Ni-NWN, NiCo LDH/Ni-NWN, and NiFe LDH/Ni-NWN at a current density of 10 mA cm^{-2} for 50 h in 1 M KOH. LSV of (b) Ni-NWN, (c) NiCo LDH/Ni-NWN, and (d) NiFe LDH/Ni-NWN before and after the experiments.

using a standard value of specific capacitance for different electrocatalysts can introduce significant errors when estimating ECSA.[54] Hence, the superior catalytic activity of NiFe LDH/Ni-NWN is not solely attributed to a higher number of active sites, as both NiCo-and NiFe-LDH nanosheets have a comparable surface area, but rather to the presence of more potent intrinsic catalytic centers with higher reaction efficiency.

The purposeful multilevel design of the 3D architectures offers several notable advantages. When compared to larger-scale sponge-type catalyst electrodes, our fine structuring demonstrates an excellent degree of miniaturization achieved with our fine structuring, requiring only a comparably thin layer of decorated nanonetwork to achieve outstanding catalytic activity. NWNs, owing to their porous and interconnected structure, provide continuous and effective routes for both mass and charge transfer, thereby enhancing the electrode performance by facilitating reaction kinetics.[33] The integrated Ni-NWN functions as a metallic 1D current collector, establishing efficient electric conduction pathways from the rear electrode surface to the hierarchically branched catalyst-solution interface. As the NWN framework simultaneously serves as the working electrode and active material, the reinforcement of the underlying Ni surface area becomes pivotal. Notably, the structural elements of classical Ni foams, such as the diameter of Ni struts, typically fall within the range of a few hundred micrometers. In contrast, our system exhibits features that are approximately 2 orders of magnitude smaller. This outstanding catalytic activity of NiFe LDH@Ni-NWN could be attributed to the presence of more potent catalytic sites with higher reaction efficiency, and the lower Tafel slope also implies that the rapid OER kinetics originate from the inclusion of Fe with its high intrinsic catalytic potency.[55,56] In detail, the significantly enhanced activity introduced upon the inclusion of Fe in the NiFe LDH/Ni-NWN electrocatalyst could be attributed to the following reasons: (i) The inclusion of Fe enhances the electrical conductivity of the Ni matrix. However, this outstanding OER performance can not only be assigned to this effect which highlights the previous findings that Fe represents the active site in the structure.[49] (ii) Although FeOOH alone does not possess enough conductivity to act as a catalyst at low overpotentials, the inclusion of Fe sites in the conductive Ni matrix demonstrates perfect energy of binding with −OH and −OOH intermediates.[57] Hence, the additional improvement in OER activity in the NiFe LDH/Ni-NWN electrocatalyst could be attributed to the activation of Ni^{3+} in the NiOOH phase at lower overpotentials due to the charge transfer from Fe. This phase is more conductive compared with the nonconductive $Ni(OH)_2$ phase. (iii) The presence of Fe^{3+} ions facilitates the diffusion of hydroxyl ions into the network.[58] The incorporation of Fe ions plays a

pivotal role in expediting the O−O coupling process on the surface of Ni, which subsequently enhances the multielectron transfer mechanism of Ni. This transformation process is intricately linked to the presence of Fe on the material's surface. The reduction in overpotential can be attributed to a sequence of oxidation steps and successive deprotonation of H_2O molecules bound to Fe^{4+} ions within the NiFe oxyhydroxide. Intriguingly, when only Fe ions are present, a notably subdued OER activity is observed, primarily due to the insulating nature of FeOOH.[59] These findings agree with the density functional theory (DFT) data that were used to determine the structural motif and identify the active metal sites for each reaction step through the calculation of the Gibbs free energy (ΔG). For instance, Guo et al. reported ΔG values of the metal sites in NiFe-LDH, which revealed that Fe has a lower ΔG value, confirming its role as the active site.[60] The results further confirmed that the inclusion of Fe into the NiOOH lattice not only affects the electronic structure but also substantially alters the chemical bonding of the metal ions and intermediates involved in the OER.

To gain deeper insights into the remarkable OER performance of NiFe LDH/Ni-NWN, EIS measurements of the three electrodes were conducted at 1.5 V vs. RHE. The Nyquist plots of the comparative samples were then fitted using the corresponding equivalent circuit, as illustrated in the inset of Figure 5d. R_s, R_{ct}, and *CPE* refer to the solution resistance, charge transfer resistance, and capacitance, respectively; the fitting values of the components are reported in Table S1. It can be clearly observed that the semicircle of the Nyquist plot, which represents the R_{ct} is much smaller in the case of NiFe LDH/Ni-NWN. The calculated R_{ct} of NiFe LDH/Ni-NWN (0.8 Ω) is smaller than that of NiCo LDH/Ni-NWN (7.2 Ω) and Ni-NWN (19.4 Ω) as reported in Table S1. The small R_{ct} confirms the fastest charge transfer at the interface and the easiest catalytic kinetics of NiFe LDH/Ni-NWN toward the OER among the other samples.[61−63] EIS measurements were conducted for the three electrocatalysts at different potentials of 1.5, 1.51, and 1.52 V vs. RHE (Figures S7−9), and the corresponding fitting parameters of the equivalent circuits are summarized in Table S2. As shown in Figure S9, the R_{ct} of the NiFe LDH/Ni-NWN decreases as the potential increases, indicating faster kinetics at higher potentials. Similar observations were acquired for Ni-NWN and NiCo LDH/Ni-NWN (Figures S7 and S8, respectively).

Long-term stability is another critical aspect of the evaluation of electrocatalysts. The robustness of the hierarchical architectures is further proven through long-term chronopotentiometry measurement at 10 mA cm^{-2} for a period of 50 h. Additionally, the LSV curves of three catalysts were compared before and after the experiments. Remarkably, both NiFe LDH/Ni-NWN and NiCo LDH/Ni-NWN showed outstanding stability of potential over 50 h during the potentiometry, while Ni-NWN revealed slight fluctuations over time, as shown in Figure 6a. The NiFe LDH/Ni-NWN achieved a potential of 1.45 V vs. RHE while delivering a current density of 10 mA cm^{-2}, retaining stability for 50 h. The LSV of the three electrocatalysts exhibited consistent behavior before and after the experiments, with a slight current attenuation observed at high potential (Figure 6b−d). Lastly, SEM and EDX measurements were conducted to investigate the morphological and structural changes of the Ni-NWN, NiCo LDH/Ni-NWN, and NiFe LDH/Ni-NWN elctrocatalysts after conducting the OER. As depicted in Figure S10, Ni-NWN retained the 3D wirelike network structure with some roughness on the surface of the wires. The accompanying EDX measurement (Figure S10c) confirmed the existence of only Ni in the sample. SEM images of NiCo LDH/Ni-NWN (Figure S11) and NiFe LDH/Ni-NWN (Figure S12) show no noticeable differences compared to the as-prepared architectures prior to the OER performance tests. This indicates that the Ni backbone and the LDH layer maintain their integrity, while the porous structure is retained even after rigorous testing, thus confirming the mechanical stability of the catalysts. The improved mechanical strength of the electrocatalysts can be attributed to their purposeful design, which incorporates a supporting layer that provides structural support to the entire network, along with sufficient interconnections between the nanowires, preventing network collapse. The EDX spectra of NiCo LDH/Ni-NWN and NiFe LDH/Ni-NWN (Figures S11c and S12c, respectively) indicate no changes in the initial composition of the electrocatalysts, which further proves the high catalytic durability toward the OER. Furthermore, after the long-term chronopotentiometry and LSV testing, XRD patterns revealed that the three electrocatalysts retained their crystal structures with no obvious new phases, as shown in Figure S13.

Generally, the OER mechanism involves three main steps: (i) water adsorption onto the surface of the electrocatalysts, (ii) water splitting into molecular oxygen, and (iii) oxygen evolution. The remarkable catalytic performance of the LDH-decorated NWN could be illustrated in light of the previously discussed results and observations. First, the NiCo and NiFe LDH nanosheets, with their distinguished layered structure, offer large intersheet spaces, which in turn facilitate the diffusion of water molecules and hydroxide ions between the layers, ensuring ultimate contact between the electroactive species involved in the OER and the active sites of the electrocatalyst. Consequently, the electrocatalysis process has larger accessible spaces not limited to the active electrode surface, which is crucial for the third step in the OER mechanism as it promotes the O_2 evolution from the electrocatalyst.[64] Figure S14 shows the O_2 evolution from the working electrode at the bottom of the cell upon increasing the potential. Second, the distinctive porous architecture of the Ni-NWN with its tortuous structure and interconnected nanoskeleton plays a critical role in increasing active surface area. Additionally, each nanowire acts as a nanocurrent collector which has direct contact with the coating LDH sheets, forming an open 3D efficiently conductive network. Such a well-designed architecture can not only preserve the catalyst's mechanical and structural stability and prevent the nanowires' collapse but also promote the charge transfer efficiency through the enhanced electrical conductivity of the metallic Ni backbone.[28,33] Noteworthy, our hierarchical paradigm of the electrocatalyst represents an efficient alternative for the commonly used assisting electrodes such as nickel foam and carbon felt without any need for conductive additives or polymer binders to mount active material on the electrode, which in turn reduces the dead volume of the electrode.[33] Third, the high valence states of Ni, Co, and Fe are the most critical to facilitate the OER, which agrees with the predictions from the Pourbaix diagram of these elements.[65−67] In alkaline media, the metal hydroxides undergo oxidation, transforming into a catalytically active oxyhydroxide form. In the case of Co and Fe, this further evolves into the oxide form, which represents the favorable metal species for electrocatalytic

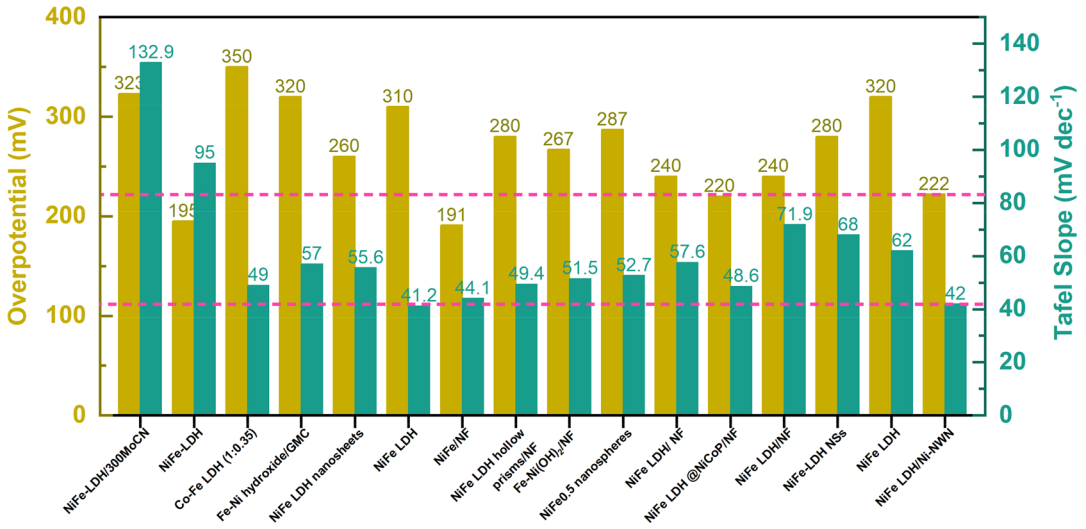

Figure 7. Comparison of the OER performance in terms of Tafel slopes and overpotentials@10 mA cm^{-2} of NiFe LDH/Ni-NWN and the recently reported non-noble metal-based electrocatalysts (refs 29, 44, and 72−83).

OER.[68,69] The transformation of the $Ni(OH)_2$/NiOOH redox couple could be approved through the visible color changes. Correspondingly, the green NiCo LDH/Ni-NWN turned into a darker color upon oxidation during the OER process (Figure S15), agreeing with the observation in previous studies.[70] A plausible mechanism, as proposed by Friebel et al., sheds light on the improved OER activity associated with the incorporation of Fe, even though Fe is known to be an insulator in FeOOH.[71] According to this mechanism, the presence of Fe ions within the lattices leads to a significantly contracted Fe−O bond length. As a result, conductivity is imparted to Fe^{3+} sites within the NiOOH lattice not by direct inclusion but by leveraging the existing conductivity of the NiOOH lattice. This suggests that the modification in effective conductivity (which varies with potential) due to Fe incorporation could contribute to the enhancement of the OER activities in Ni-based electrocatalysts, although it is not the sole contributing factor. These outstanding characteristics of the LDH-based architectures play a crucial role in enhancing the OER. Moreover, water oxidation in an alkaline medium includes a proton-coupled electron transfer. Besides the rapid diffusion of the interlayer ions in the NiCo and NiFe LDH, the redox activity of Ni, Co, and Fe enables more charges to mediate the H^+ transfer in coordination with the electron transfer reactions.[64] The previously discussed advantages of the free-standing hierarchical design of the electrocatalysts highlight their outstanding catalytic activity toward OER.

The enhanced activity of NiFe LDH/Ni-NWN toward OER in terms of overpotential and Tafel slope allowed it to perform outstandingly compared with the recently reported non-noble metal-based counterparts such as NiFe-LDH/300MoCN (323 mV, 132.9 mV dec^{-1}),[72] NiFe-LDH (195 mV, 95 mV dec^{-1}),[73] Co−Fe LDH (1:0.35) (350 mV, 49 mV dec^{-1}),[74] NiFe/NF (191 mV, 44.1 mV dec^{-1}),[75] $NiFe_{0.5}$ nanospheres (287 mV, 52.9 mV dec^{-1}),[76] and others as presented in Figure 7 and reported in detail in Table S3. As such, besides its enhanced OER activity and outstanding mechanical and electrochemical stability, NiFe LDH/Ni-NWN was synthesized via a facile and scalable approach, which is the primary prerequisite for industrialization.

CONCLUSIONS

In summary, a novel hierarchical core−shell architecture, NiFe LDH/Ni-NWN, has been developed for the OER in alkaline media. This electrocatalyst exhibited outstanding electrocatalytic activity and long-term durability toward the OER. The remarkable performance of the electrode primarily originates from the prolific engineering of the catalyst and the solid synergistic effect between the NiFe LDH sheets and the 3D interconnected Ni-NWN core. Specifically, the NiFe LDH/Ni-NWN structure facilitates not only a fast charge transfer through the metallic Ni nanowires but also a high mass transportation rate through the 3D porous network, characterized by tortuous pathways, which enhance the accessibility to the active sites. An overpotential of 222 mV was required to force a current density of 10 mA cm^{-2} for the OER using the NiFe LDH/Ni-NWN electrode. The NiFe LDH/Ni-NWN exhibited a small Tafel slope of 42 mV dec^{-1} compared to 92 and 140 mV dec^{-1} for NiCo LDH/Ni-NWN and Ni-NWN, respectively, surpassing many recently reported metal-based electrocatalysts for the OER. Furthermore, the assembled electrocatalyst proved outstanding long-term durability over 50 h, ensuring its applicability on an industrial scale. Given its simple and feasible synthetic strategy using naturally abundant and low-cost materials, coupled with the high electrocatalytic activity and long-term stability, the as-prepared NiFe LDH/Ni-NWN electrocatalyst holds tremendous promise and grand feasibility for practical OER in various industrial applications.

AUTHOR INFORMATION

Corresponding Author

Khaled M. Amin − *Department of Materials Science, Technical University of Darmstadt, Darmstadt 64287, Germany; Department of Polymer Chemistry, Atomic Energy Authority, Cairo 11787, Egypt;* orcid.org/0000-0002-7698-0098; Email: amin@ma.tu-darmstadt.de, khaledamin89@gmail.com

Authors

Kuan-Hsun Lin − *Department of Materials Science, Technical University of Darmstadt, Darmstadt 64287, Germany*

Michael Duerrschnabel − *Institute for Applied Materials - Applied Material Physics, Karlsruhe Institute of Technology, Eggenstein-Leopoldshafen 76344, Germany*

Leopoldo Molina-Luna − *Department of Materials Science, Technical University of Darmstadt, Darmstadt 64287, Germany;* orcid.org/0000-0002-9412-8093

Wolfgang Ensinger − *Department of Materials Science, Technical University of Darmstadt, Darmstadt 64287, Germany*

Notes

The authors declare no competing financial interest.

ACKNOWLEDGMENTS

The authors would like to acknowledge Christopher Gort from the Surface Science Group at TU Darmstadt for Conducting XPS measurements. The authors also thank Jean-Christophe Jaud (Strukturforschung Group, TU Darmstadt) for conducting the XRD measurements and Ulrike Kunz (Physical Metallurgy Group, TU Darmstadt) for providing assistance with the TEM measurements. Khaled M. Amin gratefully acknowledges the financial support provided by the Ministry of Higher Education & Scientific Research (Egypt) and DAAD (Germany) for his Ph.D. scholarship under the GERLS program (Grant No. 57403037).

REFERENCES

(1) Krevor, S.; de Coninck, H.; Gasda, S. E.; Ghaleigh, N. S.; de Gooyert, V.; Hajibeygi, H.; Juanes, R.; Neufeld, J.; Roberts, J. J.; Swennenhuis, F. Subsurface Carbon Dioxide and Hydrogen Storage for a Sustainable Energy Future. *Nat. Rev. Earth Environ.* **2023**, *4* (2), 102−118.

(2) Du, K.; Zhang, L.; Shan, J.; Guo, J.; Mao, J.; Yang, C.-C.; Wang, C.-H.; Hu, Z.; Ling, T. Interface Engineering Breaks Both Stability and Activity Limits of RuO2 for Sustainable Water Oxidation. *Nat. Commun.* **2022**, *13* (1), 5448.

(3) Liu, H.; Zhu, Y.; Ma, J.; Zhang, Z.; Hu, W. Recent Advances in Atomic-Level Engineering of Nanostructured Catalysts for Electrochemical CO2 Reduction. *Adv. Funct. Mater.* **2020**, *30* (17), 1910534.

(4) Li, X.; Liu, L.; Ren, X.; Gao, J.; Huang, Y.; Liu, B. Microenvironment Modulation of Single-Atom Catalysts and Their Roles in Electrochemical Energy Conversion. *Sci. Adv.* **2020**, *6* (39), 6833−6856.

(5) Dong, Z. H.; Jiang, Z.; Tang, T.; Yao, Z. C.; Xue, D.; Niu, S.; Zhang, J.; Hu, J. S. Rational Design of Integrated Electrodes for Advancing High-Rate Alkaline Electrolytic Hydrogen Production. *J. Mater. Chem. A* **2022**, *10* (24), 12764−12787.

(6) Lu, Q.; Zou, X.; Bu, Y.; Shao, Z. Structural Design of Supported Electrocatalysts for Rechargeable Zn-Air Batteries. *Energy Storage Mater.* **2023**, *55*, 166−192.

(7) Ndubuisi, A.; Abouali, S.; Singh, K.; Thangadurai, V. Recent Advances, Practical Challenges, and Perspectives of Intermediate Temperature Solid Oxide Fuel Cell Cathodes. *J. Mater. Chem. A* **2022**, *10* (5), 2196−2227.

(8) Feng, X.; Jiao, Q.; Chen, W.; Dang, Y.; Dai, Z.; Suib, S. L.; Zhang, J.; Zhao, Y.; Li, H.; Feng, C. Cactus-like NiCo2S4@NiFe LDH Hollow Spheres as an Effective Oxygen Bifunctional Electrocatalyst in Alkaline Solution. *Appl. Catal. B Environ.* **2021**, *286*, 119869.

(9) Li, W.; Tian, H.; Ma, L.; Wang, Y.; Liu, X.; Gao, X. Low-Temperature Water Electrolysis: Fundamentals, Progress, and New Strategies. *Mater. Adv.* **2022**, *3* (14), 5598−5644.

(10) Kashale, A. A.; Yi, C. H.; Cheng, K. Y.; Guo, J. S.; Pan, Y. H.; Chen, I. W. P. Binder-Free Heterostructured NiFe2O4/NiFe LDH Nanosheet Composite Electrocatalysts for Oxygen Evolution Reactions. *ACS Appl. Energy Mater.* **2020**, *3* (11), 10831−10840.

(11) Escalera-López, D.; Jensen, K. D.; Rees, N. V.; Escudero-Escribano, M. Electrochemically Decorated Iridium Electrodes with WS3-x Toward Improved Oxygen Evolution Electrocatalyst Stability in Acidic Electrolytes. *Adv. Sustain. Syst.* **2021**, *5* (11), 2000284.

(12) Park, K. W.; Kolpak, A. M. Mechanism for Spontaneous Oxygen and Hydrogen Evolution Reactions on CoO Nanoparticles. *J. Mater. Chem. A* **2019**, *7* (12), 6708−6719.

(13) Zhang, K.; Zou, R. Advanced Transition Metal-Based OER Electrocatalysts: Current Status, Opportunities, and Challenges. *Small* **2021**, *17* (37), 2100129.

(14) Wu, Z. Y.; Chen, F. Y.; Li, B.; Yu, S. W.; Finfrock, Y. Z.; Meira, D. M.; Yan, Q. Q.; Zhu, P.; Chen, M. X.; Song, T. W.; Yin, Z.; Liang, H. W.; Zhang, S.; Wang, G.; Wang, H. Non-Iridium-Based Electrocatalyst for Durable Acidic Oxygen Evolution Reaction in Proton Exchange Membrane Water Electrolysis. *Nat. Mater.* **2023**, *22* (1), 100−108.

(15) Wang, F.; Zhang, K.; Li, S.; Zha, Q.; Ni, Y. W-Doped α-Ni(OH)2Honeycomb-like Microstructures for Promoted Electrochemical Oxygen Evolution. *ACS Sustain. Chem. Eng.* **2022**, *10* (31), 10383−10392.

(16) Jiang, J.; Zhou, X. L.; Lv, H. G.; Yu, H. Q.; Yu, Y. Bimetallic-Based Electrocatalysts for Oxygen Evolution Reaction. *Adv. Funct. Mater.* **2023**, *33*, 2212160.

(17) Guo, X.; Duan, M.; Zhang, J.; Xi, B.; Li, M.; Yin, R.; Zheng, X.; Liu, Y.; Cao, F.; An, X.; Xiong, S. A General Self-Assembly Induced Strategy for Synthesizing 2D Ultrathin Cobalt-Based Compounds Toward Optimizing Hydrogen Evolution Catalysis. *Adv. Funct. Mater.* **2022**, *32* (51), 2209397.

(18) Prabhu, P.; Lee, J. M. Metallenes as Functional Materials in Electrocatalysis. *Chem. Soc. Rev.* **2021**, *50* (12), 6700−6719.

(19) Guo, X.; Liu, S.; Wan, X.; Zhang, J.; Liu, Y.; Zheng, X.; Kong, Q.; Jin, Z. Controllable Solid-Phase Fabrication of an Fe2O3/Fe5C2/Fe-N-C Electrocatalyst toward Optimizing the Oxygen Reduction Reaction in Zinc-Air Batteries. *Nano Lett.* **2022**, *22* (12), 4879−4887.

(20) Kong, Q.; Zhu, H.; Huang, S.; Wu, T.; Zhu, F.; Zhang, Y.; Wang, Y.; Zhang, J. Influence of Multiply Modified FeCu-Montmorillonite on Fire Safety and Mechanical Performances of Epoxy Resin Nanocomposites. *Thermochim. Acta* **2022**, *707*, 179112.

(21) Wang, Z.; Liu, W.; Hu, Y.; Guan, M.; Xu, L.; Li, H.; Bao, J.; Li, H. Cr-Doped CoFe Layered Double Hydroxides: Highly Efficient and Robust Bifunctional Electrocatalyst for the Oxidation of Water and Urea. *Appl. Catal. B Environ.* **2020**, *272*, 118959.

(22) Mu, G.; Wang, G.; Huang, Q.; Miao, Y.; Wen, D.; Lin, D.; Xu, C.; Wan, Y.; Xie, F.; Guo, W.; Zou, R. A Kinetic Control Strategy for One-Pot Synthesis of Efficient Bimetallic Metal-Organic Framework/Layered Double Hydroxide Heterojunction Oxygen Evolution Electrocatalysts. *Adv. Funct. Mater.* **2023**, *33*, 2211260.

(23) Zhu, S.; Wang, J.; Li, H.; Cai, J.; Li, Y.; Hu, J.; He, Y.; Zhou, Y. NiFe Layered Double Hydroxide Nanosheets Anchored on Cobalt Nanocrystal Matrixes as Electrocatalysts for Oxygen Evolution. *ACS Appl. Nano Mater.* **2022**, *5*, 13047−13054.

(24) Gong, L.; Yang, H.; Douka, A. I.; Yan, Y.; Xia, B. Y. Recent Progress on NiFe-Based Electrocatalysts for Alkaline Oxygen Evolution. *Adv. Sustain. Syst.* **2021**, *5* (1), 2000136.
(25) Li, X.; Liu, Y.; Sun, Q.; Huangfu, Z.; Huang, W. H.; Wang, Z.; Chueh, C. C.; Chen, C. L.; Zhu, Z. Effects of Cationic and Anionic Defects on NiFe LDH in Electrocatalytic Oxygen Evolution. *ACS Sustain. Chem. Eng.* **2022**, *10* (44), 14474−14485.
(26) Zhou, Y.; Sun, X.; Zhong, K.; Evans, D. G.; Lin, Y.; Duan, X. Control of Surface Defects and Agglomeration Mechanism of Layered Double Hydroxide Nanoparticles. *Ind. Eng. Chem. Res.* **2012**, *51* (11), 4215−4221.
(27) Yang, R.; Zhou, Y.; Xing, Y.; Li, D.; Jiang, D.; Chen, M.; Shi, W.; Yuan, S. Synergistic Coupling of CoFe-LDH Arrays with NiFe-LDH Nanosheet for Highly Efficient Overall Water Splitting in Alkaline Media. *Appl. Catal. B Environ.* **2019**, *253* (April), 131−139.
(28) Amin, K. M.; Krois, K.; Muench, F.; Etzold, B. J. M.; Ensinger, W. Hierarchical Pipe Cactus-like Ni/NiCo-LDH Core-Shell Nanotube Networks as a Self-Supported Battery-Type Electrode for Supercapacitors with High Volumetric Energy Density. *J. Mater. Chem. A* **2022**, *10* (23), 12473−12488.
(29) Zhang, H.; Li, X.; Hähnel, A.; Naumann, V.; Lin, C.; Azimi, S.; Schweizer, S. L.; Maijenburg, A. W.; Wehrspohn, R. B. Bifunctional Heterostructure Assembly of NiFe LDH Nanosheets on NiCoP Nanowires for Highly Efficient and Stable Overall Water Splitting. *Adv. Funct. Mater.* **2018**, *28* (14), 1706847.
(30) Hu, J.; Zhang, C.; Jiang, L.; Lin, H.; An, Y.; Zhou, D.; Leung, M. K. H.; Yang, S. Nanohybridization of MoS2 with Layered Double Hydroxides Efficiently Synergizes the Hydrogen Evolution in Alkaline Media. *Joule* **2017**, *1* (2), 383−393.
(31) Duan, M.; Qiu, M.; Sun, S.; Guo, X.; Liu, Y.; Zheng, X.; Cao, F.; Kong, Q.; Zhang, J. Intercalating Assembly of NiFe LDH Nanosheets/CNTs Composite as High-Performance Electrocatalyst for Oxygen Evolution Reaction. *Appl. Clay Sci.* **2022**, *216*, 106360.
(32) Amin, K. M.; Boettcher, T.; Scheuerlein, M. C.; Ensinger, W. Exotemplate-Based Fabrication of 1-Dimensional Hybrid Nanostructures for Catalysis and Sensing. Presented at World Congress on Recent Advances in Nanotechnology; 2022, DOI: 10.11159/icnnfc22.173.
(33) Amin, K. M.; Muench, F.; Kunz, U.; Ensinger, W. 3D NiCo-Layered Double Hydroxide@Ni Nanotube Networks as Integrated Free-Standing Electrodes for Nonenzymatic Glucose Sensing. *J. Colloid Interface Sci.* **2021**, *591*, 384−395.
(34) Bodhankar, P. M.; Sarawade, P. B.; Singh, G.; Vinu, A.; Dhawale, D. S. Recent Advances in Highly Active Nanostructured NiFe LDH Catalyst for Electrochemical Water Splitting. *J. Mater. Chem. A* **2021**, *9* (6), 3180−3208.
(35) Gebreslase, G. A.; Martínez-Huerta, M. V.; Lázaro, M. J. Recent Progress on Bimetallic NiCo and CoFe Based Electrocatalysts for Alkaline Oxygen Evolution Reaction: A Review. *J. Energy Chem.* **2022**, *67*, 101−137.
(36) Li, J.; Wang, L.; He, H.; Chen, Y.; Gao, Z.; Ma, N.; Wang, B.; Zheng, L.; Li, R.; Wei, Y.; Xu, J.; Xu, Y.; Cheng, B.; Yin, Z.; Ma, D. Interface Construction of NiCo LDH/NiCoS Based on the 2D Ultrathin Nanosheet towards Oxygen Evolution Reaction. *Nano Res.* **2022**, *15* (6), 4986−4995.
(37) Dionigi, F.; Zhu, J.; Zeng, Z.; Merzdorf, T.; Sarodnik, H.; Gliech, M.; Pan, L.; Li, W. X.; Greeley, J.; Strasser, P. Intrinsic Electrocatalytic Activity for Oxygen Evolution of Crystalline 3d-Transition Metal Layered Double Hydroxides. *Angew. Chemie - Int. Ed.* **2021**, *60* (26), 14446−14457.
(38) Jiang, E.; Guo, C.; Huo, P.; Yan, Y.; Zhou, P.; Yan, Y. Vertical Growth of O-Vacancy Rich LDH Atomic Layers as OER-Sensitive Reactive Sites to Boost Overall Water Splitting on Perovskite Oxides. *ACS Sustain. Chem. Eng.* **2022**, *10* (49), 16335−16343.
(39) Qi, Z.; Weissmüller, J. Hierarchical Nested-Network Nanostructure by Dealloying. *ACS Nano* **2013**, *7* (7), 5948−5954.
(40) Palmer, D. C.; Palmer, S. E. *SingleCrystalTM: a single-crystal diffraction program for Mac and Windows*. https://crystalmaker.com/ (accessed 2023-07-15).
(41) Fairley, N.; Fernandez, V.; Richard-Plouet, M.; Guillot-Deudon, C.; Walton, J.; Smith, E.; Flahaut, D.; Greiner, M.; Biesinger, M.; Tougaard, S.; Morgan, D.; Baltrusaitis, J. Systematic and Collaborative Approach to Problem Solving Using X-Ray Photoelectron Spectroscopy. *Appl. Surf. Sci. Adv.* **2021**, *5*, 100112.
(42) Xiang, Q.; Xu, Y.; Chen, R.; Yang, C.; Li, X.; Li, G.; Wu, D.; Xie, X.; Zhu, W.; Wang, L. Electrodeposition of Pt3Sn Nano-Alloy on NiFe-Layered Double Hydroxide with "Card-House" Structure for Enhancing the Electrocatalytic Oxidation Performance of Ethanol. *ChemNanoMat* **2021**, *7* (3), 314−322.
(43) Gao, Y.; Zhao, Z.; Jia, H.; Yang, X.; Lei, X.; Kong, X.; Zhang, F. Partially Reduced Ni2+, Fe3+-Layered Double Hydroxide for Ethanol Electrocatalysis. *J. Mater. Sci.* **2019**, *54* (23), 14515−14523.
(44) Teng, X.; Guo, L.; Ji, L.; Wang, J.; Niu, Y.; Hu, Z.; Chen, Z. Self-Growing NiFe-Based Hybrid Nanosheet Arrays on Ni Nanowires for Overall Water Splitting. *ACS Appl. Energy Mater.* **2019**, *2* (8), 5465−5471.
(45) Biesinger, M. C.; Lau, L. W. M.; Gerson, A. R.; Smart, R. S. C. The Role of the Auger Parameter in XPS Studies of Nickel Metal, Halides and Oxides. *Phys. Chem. Chem. Phys.* **2012**, *14* (7), 2434−2442.
(46) Yang, H.; Wang, C.; Zhang, Y.; Wang, Q. Green Synthesis of NiFe LDH/Ni Foam at Room Temperature for Highly Efficient Electrocatalytic Oxygen Evolution Reaction. *Sci. China Mater.* **2019**, *62* (5), 681−689.
(47) Yin, P.; Wu, G.; Wang, X.; Liu, S.; Zhou, F.; Dai, L.; Wang, X.; Yang, B.; Yu, Z. Q. NiCo-LDH Nanosheets Strongly Coupled with GO-CNTs as a Hybrid Electrocatalyst for Oxygen Evolution Reaction. *Nano Res.* **2021**, *14* (12), 4783−4788.
(48) Wu, F.; Wang, Y.; Fei, S.; Zhu, G. Co-Promoted CoNi Bimetallic Nanocatalyst for the Highly Efficient Catalytic Hydrogenation of Olefins. *Nanomaterials* **2023**, *13* (13), 1939.
(49) Bates, M. K.; Jia, Q.; Doan, H.; Liang, W.; Mukerjee, S. Charge-Transfer Effects in Ni-Fe and Ni-Fe-Co Mixed-Metal Oxides for the Alkaline Oxygen Evolution Reaction. *ACS Catal.* **2016**, *6* (1), 155−161.
(50) Dionigi, F.; Zeng, Z.; Sinev, I.; Merzdorf, T.; Deshpande, S.; Lopez, M. B.; Kunze, S.; Zegkinoglou, I.; Sarodnik, H.; Fan, D.; Bergmann, A.; Drnec, J.; Araujo, J. F. de; Gliech, M.; Teschner, D.; Zhu, J.; Li, W. X.; Greeley, J.; Cuenya, B. R.; Strasser, P. In-Situ Structure and Catalytic Mechanism of NiFe and CoFe Layered Double Hydroxides during Oxygen Evolution. *Nat. Commun.* **2020**, *11* (1), 1−10.
(51) Louie, M. W.; Bell, A. T. An Investigation of Thin-Film Ni-Fe Oxide Catalysts for the Electrochemical Evolution of Oxygen. *J. Am. Chem. Soc.* **2013**, *135* (33), 12329−12337.
(52) Anantharaj, S.; Kundu, S.; Noda, S. The Fe Effect": A Review Unveiling the Critical Roles of Fe in Enhancing OER Activity of Ni and Co Based Catalysts. *Nano Energy* **2021**, *80*, 105514.
(53) Batchellor, A. S.; Boettcher, S. W. Pulse-Electrodeposited Ni-Fe (Oxy)Hydroxide Oxygen Evolution Electrocatalysts with High Geometric and Intrinsic Activities at Large Mass Loadings. *ACS Catal.* **2015**, *5* (11), 6680−6689.
(54) Boggio, R.; Carugati, A.; Trasatti, S. Electrochemical Surface Properties of Co3O4 Electrodes. *J. Appl. Electrochem.* **1987**, *17* (4), 828−840.
(55) Praveen, A. E.; Ganguli, S.; Mahalingam, V. Prudent Electrochemical Pretreatment to Promote the OER by Catalytically Inert "Iron Incorporated Metallic Ni Nanowires" Synthesizedviathe "Non-Classical" Growth Mechanism. *Nanoscale Adv.* **2020**, *2* (5), 1927−1938.
(56) Yin, S.; Tu, W.; Sheng, Y.; Du, Y.; Kraft, M.; Borgna, A.; Xu, R. A Highly Efficient Oxygen Evolution Catalyst Consisting of Interconnected Nickel-Iron-Layered Double Hydroxide and Carbon Nanodomains. *Adv. Mater.* **2018**, *30* (5), 1705106.
(57) Friebel, D.; Louie, M. W.; Bajdich, M.; Sanwald, K. E.; Cai, Y.; Wise, A. M.; Cheng, M. J.; Sokaras, D.; Weng, T. C.; Alonso-Mori, R.; Davis, R. C.; Bargar, J. R.; Nørskov, J. K.; Nilsson, A.; Bell, A. T. Identification of Highly Active Fe Sites in (Ni,Fe)OOH for

Electrocatalytic Water Splitting. *J. Am. Chem. Soc.* **2015**, *137* (3), 1305−1313.
(58) Pourfarzad, H.; Shabani-Nooshabadi, M.; Ganjali, M. R.; Kashani, H. Synthesis of Ni-Co-Fe Layered Double Hydroxide and Fe2O3/Graphene Nanocomposites as Actively Materials for High Electrochemical Performance Supercapacitors. *Electrochim. Acta* **2019**, *317*, 83−92.
(59) Qiao, C.; Usman, Z.; Cao, T.; Rafai, S.; Wang, Z.; Zhu, Y.; Cao, C.; Zhang, J. High-Valence Ni and Fe Sites on Sulfated NiFe-LDH Nanosheets to Enhance O-O Coupling for Water Oxidation. *Chem. Eng. J.* **2021**, *426*, 130873.
(60) Guo, P. F.; Yang, Y.; Wang, W. J.; Zhu, B.; Wang, W. T.; Wang, Z. Y.; Wang, J. L.; Wang, K.; He, Z. H.; Liu, Z. T. Stable and Active NiFeW Layered Double Hydroxide for Enhanced Electrocatalytic Oxygen Evolution Reaction. *Chem. Eng. J.* **2021**, *426*, 130768.
(61) Nie, J.; Hong, M.; Zhang, X.; Huang, J.; Meng, Q.; Du, C.; Chen, J. 3D Amorphous NiFe LDH Nanosheets Electrodeposited on: In Situ Grown NiCoP@NC on Nickel Foam for Remarkably Enhanced OER Electrocatalytic Performance. *Dalt. Trans.* **2020**, *49* (15), 4896−4903.
(62) Galal, A.; Amin, K. M.; Atta, N. F.; Abd El-Rehim, H. A. Protective Ability of Graphene Prepared by γ-Irradiation and Impregnated with Organic Inhibitor Applied on AISI 316 Stainless Steel. *J. Alloys Compd.* **2017**, *695*, 638−647.
(63) Atta, N. F.; Amin, K. M.; Abd El-Rehim, H. A.; Galal, A. Graphene Prepared by Gamma Irradiation for Corrosion Protection of Stainless Steel 316 in Chloride Containing Electrolytes. *RSC Adv.* **2015**, *5* (88), 71627−71636.
(64) Jiang, J.; Zhang, A.; Li, L.; Ai, L. Nickel-Cobalt Layered Double Hydroxide Nanosheets as High-Performance Electrocatalyst for Oxygen Evolution Reaction. *J. Power Sources* **2015**, *278*, 445−451.
(65) Beverskog, B.; Puigdomenech, I. Revised Pourbaix Diagrams for Nickel at 25−300°c. *Corros. Sci.* **1997**, *39* (5), 969−980.
(66) Bloor, L. G.; Molina, P. I.; Symes, M. D.; Cronin, L. Low PH Electrolytic Water Splitting Using Earth-Abundant Metastable Catalysts That Self-Assemble in Situ. *J. Am. Chem. Soc.* **2014**, *136* (8), 3304−3311.
(67) Perry, S. C.; Gateman, S. M.; Stephens, L. I.; Lacasse, R.; Schulz, R.; Mauzeroll, J. Pourbaix Diagrams as a Simple Route to First Principles Corrosion Simulation. *J. Electrochem. Soc.* **2019**, *166* (11), C3186−C3192.
(68) Trotochaud, L.; Young, S. L.; Ranney, J. K.; Boettcher, S. W. Nickel-Iron Oxyhydroxide Oxygen-Evolution Electrocatalysts: The Role of Intentional and Incidental Iron Incorporation. *J. Am. Chem. Soc.* **2014**, *136* (18), 6744−6753.
(69) Moysiadou, A.; Lee, S.; Hsu, C. S.; Chen, H. M.; Hu, X. Mechanism of Oxygen Evolution Catalyzed by Cobalt Oxyhydroxide: Cobalt Superoxide Species as a Key Intermediate and Dioxygen Release as a Rate-Determining Step. *J. Am. Chem. Soc.* **2020**, *142* (27), 11901−11914.
(70) Stern, L. A.; Hu, X. Enhanced Oxygen Evolution Activity by NiOx and Ni(OH)2 Nanoparticles. *Faraday Discuss.* **2014**, *176* (0), 363−379.
(71) Friebel, D.; Louie, M. W.; Bajdich, M.; Sanwald, K. E.; Cai, Y.; Wise, A. M.; Cheng, M. J.; Sokaras, D.; Weng, T. C.; Alonso-Mori, R.; Davis, R. C.; Bargar, J. R.; Nørskov, J. K.; Nilsson, A.; Bell, A. T. Identification of Highly Active Fe Sites in (Ni,Fe)OOH for Electrocatalytic Water Splitting. *J. Am. Chem. Soc.* **2015**, *137* (3), 1305−1313.
(72) Du, Y.; Zhang, Y.; Pu, X.; Fu, X.; Li, X.; Bai, L.; Chen, Y.; Qian, J. Synthesis of Bifunctional NiFe Layered Double Hydroxides (LDH)/Mo-Doped g-C3N4 Electrocatalyst for Efficient Methanol Oxidation and Seawater Splitting. *Chemosphere* **2023**, *312*, 137203.
(73) Praveen Kumar, M.; Sasikumar, M.; Arulraj, A.; Rajasudha, V.; Murugadoss, G.; Kumar, M. R.; Gouse Peera, S.; Mangalaraja, R. V. NiFe Layered Double Hydroxide Electrocatalyst Prepared via an Electrochemical Deposition Method for the Oxygen Evolution Reaction. *Catalysts* **2022**, *12* (11), 1470.
(74) Hu, Y.; Liu, W.; Jiang, K.; Xu, L.; Guan, M.; Bao, J.; Ji, H.; Li, H. Constructing a CeO2-: X@CoFe-Layered Double Hydroxide Heterostructure as an Improved Electrocatalyst for Highly Efficient Water Oxidation. *Inorg. Chem. Front.* **2020**, *7* (22), 4461−4468.
(75) Jin, J.; Xia, J.; Qian, X.; Wu, T.; Ling, H.; Hu, A.; Li, M.; Hang, T. Exceptional Electrocatalytic Oxygen Evolution Efficiency and Stability from Electrodeposited NiFe Alloy on Ni Foam. *Electrochim. Acta* **2019**, *299*, 567−574.
(76) Chen, M.; Lu, S.; Fu, X. Z.; Luo, J. L. Core-Shell Structured NiFeSn@NiFe (Oxy)Hydroxide Nanospheres from an Electrochemical Strategy for Electrocatalytic Oxygen Evolution Reaction. *Adv. Sci.* **2020**, *7* (10), 1903777.
(77) Yu, L.; Yang, J. F.; Guan, B. Y.; Lu, Y.; Lou, X. W. D. Hierarchical Hollow Nanoprisms Based on Ultrathin Ni-Fe Layered Double Hydroxide Nanosheets with Enhanced Electrocatalytic Activity towards Oxygen Evolution. *Angew. Chemie - Int. Ed.* **2018**, *57* (1), 172−176.
(78) Liu, J.; Zheng, Y.; Wang, Z.; Lu, Z.; Vasileff, A.; Qiao, S. Z. Free-Standing Single-Crystalline NiFe-Hydroxide Nanoflake Arrays: A Self-Activated and Robust Electrocatalyst for Oxygen Evolution. *Chem. Commun.* **2018**, *54* (5), 463−466.
(79) Bi, Y.; Cai, Z.; Zhou, D.; Tian, Y.; Zhang, Q.; Zhang, Q.; Kuang, Y.; Li, Y.; Sun, X.; Duan, X. Understanding the Incorporating Effect of Co2+/Co3+ in NiFe-Layered Double Hydroxide for Electrocatalytic Oxygen Evolution Reaction. *J. Catal.* **2018**, *358*, 100−107.
(80) Babar, P.; Lokhande, A.; Karade, V.; Pawar, B.; Gang, M. G.; Pawar, S.; Kim, J. H. Bifunctional 2D Electrocatalysts of Transition Metal Hydroxide Nanosheet Arrays for Water Splitting and Urea Electrolysis. *ACS Sustain. Chem. Eng.* **2019**, *7* (11), 10035−10043.
(81) Wang, L.; Huang, X.; Xue, J. Graphitic Mesoporous Carbon Loaded with Iron-Nickel Hydroxide for Superior Oxygen Evolution Reactivity. *ChemSusChem* **2016**, *9* (14), 1835−1842.
(82) Yang, H.; Luo, S.; Bao, Y.; Luo, Y.; Jin, J.; Ma, J. In Situ Growth of Ultrathin Ni-Fe LDH Nanosheets for High Performance Oxygen Evolution Reaction. *Inorg. Chem. Front.* **2017**, *4* (7), 1173−1181.
(83) Zhou, J.; Yu, L.; Zhu, Q.; Huang, C.; Yu, Y. Defective and Ultrathin NiFe LDH Nanosheets Decorated on V-Doped Ni3S2 Nanorod Arrays: A 3D Core-Shell Electrocatalyst for Efficient Water Oxidation. *J. Mater. Chem. A* **2019**, *7* (30), 18118−18125.